AIAA SciTech
4-8 January 2016, San Diego, California, USA
AIAA Atmospheric Flight Mechanics Conference

System Identification of a Small Flexible Aircraft

Harald Pfifer*
University of Minnesota, Minneapolis, MN 55455, USA
Brian Danowsky †
Systems Technology Inc., Hawthorne, CA 90250, USA

This paper describes system identification of a light weight, high aspect-ratio flying-wing type aircraft. For this aircraft, complex flexible structure poses challenges in correctly identifying and validating the aircraft structural modes. Also, structural deformation coupled with unsteady aerodynamics in flight makes aerodynamic characterization difficult. The aircraft is identified in flight with inputs carefully selected to excite the dynamic modes of interest. In this study, the lightly damped structural modes are identified based on spectral analysis. The aerodynamic parameters are estimated using prediction error methods. The results of the estimation are validated on data at different flight conditions, as well as by comparison to subspace based black box models. A focus of the paper lies on providing useful insights and lessons learned during the flight test campaign.

I. Introduction

Aeroservoelastic research aids the design of lightweight, slender wings, whose flexibility can increase aircraft endurance and maneuverability. These modifications can achieve fuel efficiency gains and extended range due to reduced air resistance. In turn, the cost of operation can be reduced. However, the high flexibility and significant deformation in flight exhibited by these aircraft increases the interaction between the aerodynamics and structural dynamics. This can result in adverse handling qualities and may even lead to dynamic instability. This instability, called flutter, can destroy the aircraft if left uncontrolled. Hence, accurate models are required to predict and control this dangerous phenomena.

This paper presents an approach to identify a model of flexible aircraft dynamics from flight data suitable for control design of an active flutter suppression controller. Such an initial flutter suppression control design based on the models obtained in this paper is presented in Ref. 1. The test vehicle is a 3 m wing span unmanned aerial vehicle (UAV), denoted Sköll, which was build at University of Minnesota as part of the Performance Adaptive Aeroelastic Wing (PAAW) program. It is an important part of the PAAW project to provide all the acquired data and models to the community. Hence, all flight data and identified models are available on the project website `www.paaw.net`. The main contribution of the paper is to identify a linear parameter varying model of the flexible aircraft suitable for control design. The approach is based on estimation of physical meaningful parameters. It provides a consistent state vector over the flight envelope. It also allows exploiting knowledge of the model structure. Specifically in this paper, the model structure for the identification is taken from Ref. 2, see Section III. It is based on the aeroelastic modeling approach proposed in Refs. 3, 4. As the parameter estimation is based on a nonconvex optimization problem, it is highly dependent on good initial values and a suitable model structure. Some parameters of the model, i.e. the structural modes, can be identified separately by using a modal identification approach on ground test data as described in Ref. 5. The structural modes, and especially their frequencies, have a large impact on the dynamical behavior of the aircraft. In order to judge the quality of the parametric model, various different black box approaches are used to identify linear, time invariant models at fixed flight conditions. An overview of the used system identification algorithms is given in Section II. Several flight tests at different flight conditions and with different excitation signals have been conducted to provide a rich data set for the identification, see Section IV. Unfortunately, the aircraft was destroyed in one of these flight tests, so that

*Post-Doctoral Associate, Aerospace Engineering and Mechanics Department, email: hpfifer@umn.edu
†Principal Research Engineer, email: bdanowsky@systemstech.com

a full test campaign could not be completed. Still, the obtained data provides valuable insights and lessons for the identification procedure of flexible aircraft.

System identification of classical, rigid aircraft is a well established field, see for instance Refs. 6–8. In contrast, only limited literature exists on the identification process for flexible aircraft. In Ref. 9, the flexible modes of a large wide-body transport aircraft have been identified. The considered aircraft had a negligible coupling between the rigid body dynamics and the flexible dynamics, so that both could be treated independently. This is in stark contrast to the aircraft considered in this paper, which is highly coupled. Even at low airspeeds, the aircraft has no clear distinction between classical rigid body dynamics and flexible effects. An aircraft with similar coupling was studied in Refs. 10,11. The high aspect ratio glider that was the focus of the research in Ref. 11 was equipped with an abundance of sensors, both accelerometers as well as strain gauges. The aircraft in this paper only has a limited amount of accelerometers, which makes the identification of the structural modes a difficult task.

II. System Identification Algorithms

The system identification objective is to build mathematical models of dynamic systems based on data observations. The construction of these models involves three entities: (i) recorded experimental input-output data, (ii) selection of a mathematical modeling framework, and (iii) choice of system identification algorithms that will yield the best model fitting the observed data.[12] In this section the identification algorithms used in this paper are briefly discussed. From flight test time series $\{u(t_k)\}_1^N$ and $\{y(t_k)\}_1^N$ of the input and corresponding output, respectively, are available. Depending on the choice of model structure $\mathcal{M}$, e.g. state space representations, transfer functions or specific physical models, the model is parameterized by a vector θ. Formally, the set of models is defined as

$$\mathcal{M}^* = \{\mathcal{M}(\theta)|\theta \in \mathcal{T}\}, \tag{1}$$

where $\mathcal{T}$ is the set of all possible parameters.

The spectral content $\{U(j\omega_k)\}_1^N$ and $\{Y(j\omega_k)\}_1^N$ of the time histories $\{u(t_k)\}_1^N$ and $\{y(t_k)\}_1^N$ can be calculated using Fast Fourier Transformation (FFT). Several data smoothing options, developed and refined through practical experience, are available for smoothing and reducing the myriad of data points typically obtained during spectral analysis. In this paper, frequency windowing[12] is used for smoothing. Specifically, the frequency response data at a certain frequency ω_j is computed from a weighted average of a frequency interval around ω_j. The size of the frequency interval is the window width. It offers a trade off between the variance and the bias of the response data. A wide width leads to small variance, as many different frequencies are weighted together. However, for the same reasons it increases the bias, as frequencies far from ω_j contribute to the response.

A. CFDD Output-Only Modal Identification

The Curve-Fitting Frequency Domain Decomposition (CFDD) has been applied successfully to both simulated and actual flight test data in previous work.[5] The classical approach used to identify modal characteristics of a vibrating system is based on picking the peaks in the power-spectral density diagram.[13] For well separated modes, the technique can give a reasonable estimation of natural frequencies and mode shapes but when the modes are closely spaced, the estimation of the mode shapes and natural frequencies can become heavily biased.[14] Also, the autospectra of the output signals do not provide sufficient information to estimate accurate normal modes of vibration.[5] The cross-spectra magnitude and phase along with coherence are also equally important to provide an accurate estimation of the normal modes. However, using classical frequency domain analysis for picking dominant peaks imposes a great deal of practical difficulties. All cross-spectral density plots need to be investigated and this becomes impractical when there are many measurements to deal with. To remedy this issue, Refs. 14, 15 suggested the use of the Singular Value Decomposition (SVD) of the power spectral-density matrix. In this approach, the power spectral-density matrix is first built from all measured outputs containing diagonal elements with the autospectral density of each output and off-diagonal elements with the cross-spectral densities of individual outputs. The power spectral-density matrix at each frequency of interest is then decomposed by applying SVD to the matrix. The Frequency Domain Decomposition (FDD) theory states that the first singular vector corresponding to the first singular value is an estimation of the mode shape corresponding to a single degree of freedom system. With the identified

autospectral density function, the natural frequencies and the damping ratios can easily be estimated. The CFDD technique is a method to directly identify the natural frequencies and the damping ratios from the Single Degrees of Freedom (SDOF) spectrum of measured outputs. As the name indicates, this method fits each SDOF spectrum with a second order transfer function and the roots of the denominator of the identified transfer function provides the estimation of the natural frequencies and the damping ratios of the individual SDOF vibration modes.

B. Prediction Error Methods

At the core of each system identification algorithm is the minimization of the difference between the experimental input-output data and the input-output data of a model $\mathcal{M}(\theta)$. A classical error metric in literature is the so-called prediction error.[12] For a particular model $\mathcal{M}(\theta)$ at a time instance t_i, it is given by

$$e(t_i, \theta) = y(t_i) - \hat{y}(t_i, \theta). \tag{2}$$

Considering a time series $\{u(t_k)\}_1^N$ and $\{y(t_k)\}_1^N$, the norm of the prediction error over the sum of all data points can be obtained as $\frac{1}{N}\sum_{i=1}^{N}\frac{1}{2}e(t_i,\theta)^T e(t_i,\theta)$. Note that in this specific case the quadratic norm is considered, but in general any norm can be used. Additionally, frequency or time weighting could in principle be included in a prediction error method. For simplicity, weightings will not be considered in this paper. The error can also be defined in the frequency domain by using the Fourier transform of $y(t)$ and $\hat{y}(t)$.

Assuming a model structure $\mathcal{M}^*$, as defined in Equation (1), the objective of the parameter estimation algorithm is to minimize the prediction error over the available parameters θ. The optimal estimate $\hat{\theta}$ of the parameter θ is then defined by

$$\hat{\theta} = \arg\min_{\theta\in\mathcal{T}} \frac{1}{N}\sum_{i=1}^{N}\frac{1}{2}e(t_i,\theta)^T e(t_i,\theta). \tag{3}$$

Many variants of this approach exist in literature which are summarized in Ref. 12 under the general term prediction error identification methods. In a general parameter estimation problem, the model structure $\mathcal{M}^*$ is a nonlinear function of θ. Hence, there is no analytical method to minimize the norm of the prediction error. Therefore, iterative search algorithms need to be applied. Newton algorithms, i.e. iterative methods based on the evaluation of the function, its gradient and its Hessian, are used in the present work. These are implemented in the System Identification Toolbox of MATLAB. Naturally, these algorithm can only find a local minimum and are highly dependent on good initial values for the parameter θ.

C. Subspace Methods

In the special case that the model structure is assumed to be linear time invariant, i.e.

$$\begin{aligned} x(t+1) &= Ax(t) + Bu(t) \\ y(t) &= Cx(t) + Du(t), \end{aligned} \tag{4}$$

subspace based methods can be applied. These approaches are also well suited to handle multivariable systems. Unlike the previously described prediction error methods, subspaces methods can be solved directly by a series of linear least squares problems. Hence, they require no iterative solutions. The basic principle behind subspace methods can be described in the following way: If the state vector x is known at each time step, the problem of finding the matrices A, B, C and D in Equation (4) is a simple linear least squares problem. Basic realization theory can be used to get an estimate of the state vector.

Subspace methods consist of a two step procedure. In the first step, the observability matrix of the system is estimated based on the input-output behavior $\{u(t_k)\}_1^N$ and $\{y(t_k)\}_1^N$. This determines the matrices C and A. Assuming the system order is known a priori this amounts to solving a linear least squares problem. With A and C known it is easy to see that B and D only depend linearly on the input/ouput data. Thus, the second step contains solving another linear least squares problems to obtain B and D. In the present work the algorithm N4SID proposed in Ref. 16 is used. This algorithm is implemented in the MATLAB System Identification Toolbox. Details of subspace methods are found in Ref. 12.

III. Test Vehicle

A. Aircraft Description

The aircraft under consideration in this paper is denoted Sköll and is of the mini MUTT (Multi Utility Technology Testbed) type built at the University of Minnesota. It is a remote-piloted flying wing aircraft which closely resembles Lockheed Martin's Body Freedom Flutter vehicle.[17] The key distinction between both aircraft is that the mini MUTT follows a modular design philosophy similar to the X-56 MUTT aircraft. It features a common rigid center body and interchangeable wings of varying flexibility. This modular approach allows testing several wing configurations at a low cost. Sköll in the considered configuration has a mass of $m = 6.69\,\mathrm{kg}$, a pitch inertia of $I_{yy} = 0.464\,\mathrm{kg\,m^2}$, a mean chord of $\bar{c} = 0.321\,\mathrm{m}$ and a reference area of $S = 1.05\,\mathrm{m^2}$.

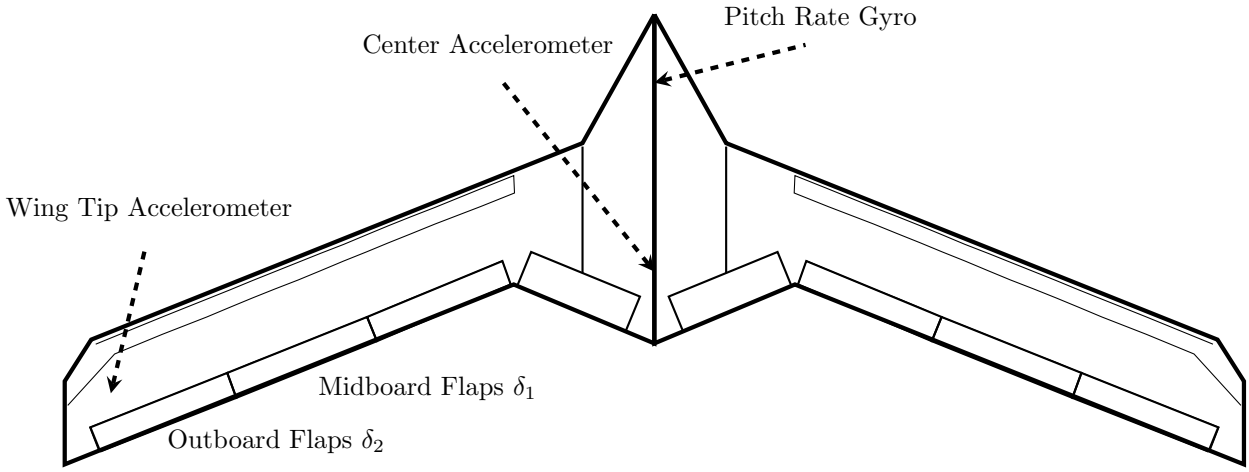

Figure 1. Mini MUTT Vehicle

The basic aircraft configuration of the mini MUTT vehicle with location of sensors and control surfaces is presented in Fig. 1. The aircraft has 8 control surfaces and 9 sensors available for control. Sensor measurements include gyros and accelerometers located on various locations of the center body and the wing. The angular rates are obtained by an inertial measurement unit (IMU) that includes a 50 Hz low-pass filter. The accelerometer signals are filtered by an analog first order low-pass filter with a bandwidth of 35 Hz. Longitudinal control is achieved by deflection of the midboard flaps; roll control by the inboard flaps. Additionally, outboard flaps will be used to suppress flutter. The goal of this system identification work is to obtain a model suitable for designing a pitch tracker and flutter suppression controller. Therefore, only the midboard and outboard flaps are excited in the experiments. All flaps are actuated by the same electrical actuators. Their dynamics have been identified via frequency-domain identification techniques using a chirp input signal. The resulting actuator model is the following second order system

$$G_{act} = \frac{96710}{s^2 + 840s + 96710} \tag{5}$$

B. Parametric Model

The parametric model of the aircraft was developed in Ref 2 and is based on the approach proposed in Ref. 3. A brief overview of the model is given in this section. Specifically, the main focus here lies on the parameters that will be updated with flight test data. A detailed description of the general model can be found in Ref 2. Note that the presented model only considers the longitudinal dynamics for straight and level flight under small elastic deformations.

The model contains four rigid states, namely the forward velocity u, the angle of attack α, the pitch angle θ and the pitch rate q. Additionally, the first three symmetric free vibration modes were used in the development of the dynamic model. Specifically, these are the first symmetric wing bending, the first symmetric wing torsion and the second symmetric wing bending mode. The modes are described by their modal displacements

$\{\eta_i\}_{i=1}^3$ and velocity $\{\dot{\eta}_i\}_{i=1}^3$. Hence, the state vector is given by $x = [u, \alpha, \theta, q, \eta_1, \dot{\eta}_1, \eta_2, \dot{\eta}_2, \eta_3, \dot{\eta}_3]^T$. The model is given in its state space representation in dependence on the flight speed V by

$$\begin{aligned} \dot{x} &= A(V)x + B(V)u \\ y &= C(V)x + D(V)u, \end{aligned} \tag{6}$$

where the output $y = [q, a_{z,cg}, a_{z,RW}]$ is the pitch rate, the vertical acceleration at the center of gravity and the vertical acceleration on the right wing tip. The aircraft has a fore and an aft accelerometer on the wing tip. In the present paper, the averaged value of these two accelerometers is considered as the output of the system. The input u contains the midboard flap deflection δ_1 and the outboard flap deflection δ_2, i.e. $u = [\delta_1, \delta_2]^T$. The state space matrices have the following structure, where the entires X_i, Z_i, M_i and $\Xi_{k,i}$ for $i \in \{u, \alpha, q, \eta_1, \dot{\eta}_1, \eta_3, \dot{\eta}_3, \delta_1, \delta_2\}$ and $k = 1, 2, 3$ are the dimensional aerodynamic derivatives. The entries ω_k and ζ_k are the frequency and damping of the k^{th} structural mode and g is the gravitational acceleration.

$$A = \begin{bmatrix} X_u & X_\alpha & -g & X_q & 0 & 0 & \dots & 0 & 0 \\ Z_u/V & Z_\alpha/V & 0 & 1+Z_q/V & Z_{\eta_1}/V & Z_{\dot{\eta}_1}/V & \dots & Z_{\eta_3}/V & Z_{\dot{\eta}_3}/V \\ 0 & 0 & 0 & 1 & 0 & 0 & \dots & 0 & 0 \\ M_u & M_\alpha & 0 & M_q & M_{\eta_1} & M_{\dot{\eta}_1} & \dots & M_{\eta_3} & M_{\dot{\eta}_3} \\ 0 & 0 & 0 & 0 & 0 & 1 & \dots & 0 & 0 \\ 0 & \Xi_1\alpha & 0 & \Xi_1 q & \Xi_{1\eta_1} - \omega_1^2 & \Xi_{1\dot{\eta}_1} - 2\omega_1\zeta_1 & \dots & \Xi_{1\eta_3} & \Xi_{1\dot{\eta}_3} \\ \vdots & \vdots & \vdots & \vdots & \vdots & \vdots & \dots & \vdots & \vdots \\ 0 & 0 & 0 & 0 & 0 & 1 & \dots & 0 & 0 \\ 0 & \Xi_3\alpha & 0 & \Xi_3 q & \Xi_{3\eta_1} & \Xi_{3\dot{\eta}_1} & \dots & \Xi_{3\eta_3} - \omega_3^2 & \Xi_{3\dot{\eta}_3} - 2\omega_3\zeta_3 \end{bmatrix} \tag{7}$$

$$B = \begin{bmatrix} X_{\delta_1} & X_{\delta_2} \\ Z_{\delta_1}/V & Z_{\delta_2}/V \\ 0 & 0 \\ M_{\delta_1} & M_{\delta_2} \\ 0 & 0 \\ \Xi_{1\delta_1} & \Xi_{1\delta_2} \\ \vdots & \vdots \\ 0 & 0 \\ \Xi_{3\delta_1} & \Xi_{3\delta_2} \end{bmatrix} \tag{8}$$

The sensor signals can be obtained by superposition of the elastic deformations with the rigid body motion in terms of their mode shapes. This allows specifying the accelerations and angular velocities of any point on the aircraft as a linear function of the states. A detailed description of this approach is given in Ref. 4. It is used to obtain C and D in Equation (6) based on the mode shapes of the aircraft. They are obtained by ground vibration test[18] and the modal identification presented in Section V.

The initial values of the aerodynamic coefficients are computed by a vortex lattice method.[2] Only a subset of them will be updated during the system identification. Specifically, only the coefficients associated with the short period and the first flexible mode are considered in the parameter estimation. These are the following 18 coefficients: Z_i, M_i, Ξ_1, i for $i \in \{\alpha, q, \eta_1, \dot{\eta}_1, \delta_1, \delta_2\}$. The flight data duration is too short to effectively capture the low frequency phugoid mode. Hence, coefficients associated with this mode are kept at the values obtained by computational aerodynamics, i.e. the first row and column of A and the first row of B. The two higher frequency flexible modes are also outside the spectrum of the excitation signal and the sampling rate. Therefore, the coefficients corresponding to these modes are also not altered by the parameter estimation, i.e. the last four rows and columns of A and the last four rows of B. The structural frequencies ω_2 and ω_3 of these two modes are, however, updated by the modal identification of the ground vibration test data.

Instead of working with the dimensional coefficients, the dimensionless ones are used. This allows updating the coefficients with flight data at different flight conditions. The coefficients are made dimensionless in the

following way with $q = \frac{1}{2}\rho V^2$ being the dynamic pressure and ρ the air density.

$$\begin{array}{lll} C_{M\alpha} = M_\alpha \frac{I_{yy}}{qS\bar{c}} & C_{L\alpha} = -Z_\alpha \frac{m}{qS} & C_{Q1\alpha} = \Xi_{1\alpha} \frac{1}{qS\bar{c}} \\ C_{Mq} = M_q \frac{2VI_{yy}}{qS\bar{c}^2} & C_{Lq} = -Z_q \frac{2Vm}{qS\bar{c}} & C_{Q1q} = \Xi_{1q} \frac{V}{qS\bar{c}} \\ C_{M\delta_1} = M_{\delta_1} \frac{I_{yy}}{qS\bar{c}} & C_{L\delta_1} = -Z_{\delta_1} \frac{m}{qS} & C_{Q1\delta_1} = \Xi_{1\delta_1} \frac{1}{qS\bar{c}} \\ C_{M\delta_2} = M_{\delta_2} \frac{I_{yy}}{qS\bar{c}} & C_{L\delta_2} = -Z_{\delta_2} \frac{m}{qS} & C_{Q1\delta_2} = \Xi_{1\delta_2} \frac{1}{qS\bar{c}} \\ C_{M\eta_1} = M_{\eta_1} \frac{I_{yy}}{qS\bar{c}} & C_{L\eta_1} = -Z_{\eta_1} \frac{m}{qS} & C_{Q1\eta_1} = \Xi_{1\eta_1} \frac{1}{qS\bar{c}} \\ C_{M\dot{\eta}_1} = M_{\dot{\eta}_1} \frac{VI_{yy}}{qS\bar{c}} & C_{L\dot{\eta}_1} = -Z_{\dot{\eta}_1} \frac{Vm}{qS} & C_{Q1\dot{\eta}_1} = \Xi_{1\dot{\eta}_1} \frac{V}{qS\bar{c}} \end{array} \tag{9}$$

IV. Flight Test

A. Flight experiments

The initial test campaign for system identification of the Sköll aircraft consists of five flights at four flight conditions and with two different excitation signals. In addition, a ground vibration test (GVT)[18] was performed and the modal identification approach in Section II was applied to obtain the pure structural modes of the aircraft. All test flights were performed open loop with the pilot controlling the aircraft through the inboard and midboard flaps for roll and pitch control, respectively. The excitation signals were injected on the midboard and outboard flaps. The goal of the system identification is to obtain models suitable for designing suppression control of the body freedom flutter mode. Hence, only symmetric excitation signals are used and only the longitudinal dynamics are identified. An overview of the experiments is given in Tab. 1.

Table 1. Flight test conditions

Flight Number	Flight Speed [m/s]	Test Signal	Time Segment	Test Date
	0	GVT	[0, 120]	8/18/15
Sköll 3	20	3-2-1-1	[540 580]	7/2/15
Sköll 9a	23	Chirp	[205 237]	8/9/15
Sköll 9b	23	3-2-1-1	[260 297]	8/9/15
Sköll 12	26	Chirp	[296 314],[340,365]	8/25/15
Sköll 13	30	Flutter		8/25/15

The two excitation signals that were used in the flight tests are a chirp signal going from 0.5 Hz to 8 Hz and a 3-2-1-1 signal. Both signals are depicted in Fig. 2 both their time history, as well as their power spectra. As can be seen in the figure, the chirp provides a much cleaner power spectrum over the frequency range of interest. Specifically, the 3-2-1-1 are not sufficiently exciting the higher frequencies to clearly identify the flexible modes of the system. Hence, the focus of this paper is on the two data sets with the chirp signals (i.e. Sköll 9a and 12). The 3-2-1-1 flights will only be used as validation data. The ground vibration test also used a chirp excitation from 1 Hz to 35 Hz. The aircraft was excited using a shaker in a similar setup as described in Ref. 19.

Sköll flight 3 consists of a combined 3-2-1-1 of both midboard and outboard flap followed by individual 3-2-1-1's on midboard and outboard flap. Sköll flight 9b uses the same sequence of midboard flap followed by outboard flap but repeats the sequence twice. For Sköll flights 9a and 12, the chirp excitation was first put on the midboard flap and then after a short break on the outboard flap. The only difference between the two chirp excitation is that at the higher airspeed, flight 12, the chirp gets a reduced amplitude at higher frequencies in order to avoid putting excess energy into the lightly damped, flexible mode. Unfortunately, the aircraft was destroyed during a flight test, i.e. Sköll flight 13, before more data could have been acquired, see Fig. 3. Data on flight 13 could not be recovered. Based on the recollection of the test engineer, who had a speed indicator downlink, the flutter speed is estimated to be approximately 30 m/s.

B. Lessons Learned

In this section some important lessons learned from the flight test campaign in regard to the excitation signals are presented. It was already mentioned in the previous section (see Fig. 2) that the 3-2-1-1 does not

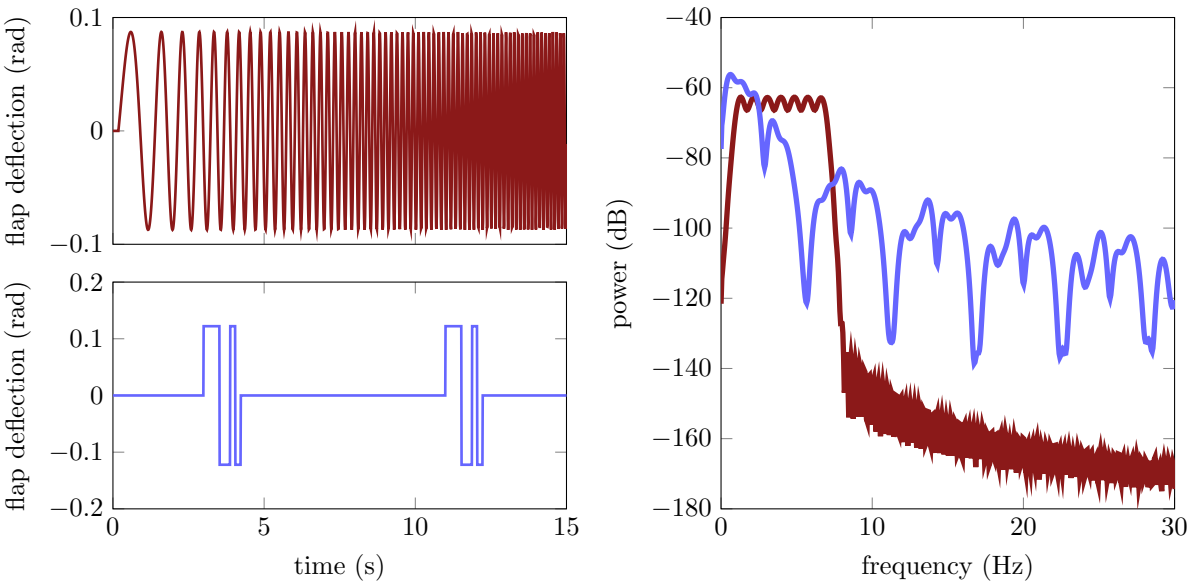

(a) Excitation Signals

(b) Power Sepctrum

Figure 2. Comparison of Chirp (——) and 3-2-1-1 Excitation (——)

Figure 3. Flutter of Sköll during Flight 13

excite the dynamics sufficiently. In theory, the chirp signal provides a very good excitation spectrum. Still, care has to be taken in the practical execution. For a clear excitation, it is important that the chirp starts in a trim and ends in a trim. In Sköll flight 9a, the first chirp was initiated too early by the pilot. The aircraft was not yet in a straight and level condition. This resulted in washing out the low frequency content of the excitation by the pilot inputs to steer the aircraft in the trim condition. Additionally, the second chirp was cut short by the pilot, as it is difficult to see from the ground when the automated signal has completed. As a consequence, an additional downlink has been implemented for subsequent flight tests that shows the test engineer the percentage of the remaining experiment duration.

It is further important to analyze the flight data carefully before applying system identification approaches. The coherency spectrum κ_{yu} between the input and the output signal provides a good metric for how correlated the signals are, see Ref. 12 for details. It is defined by of cross spectrum Φ_{yu} and the product of the individual signal spectra Φ_y and Φ_u as given by

$$\kappa_{yu} = \sqrt{\frac{|\Phi_{yu}(\omega)|}{\Phi_y(\omega)\Phi_u(\omega)}}. \tag{10}$$

The coherency spectrum can take values between 0 and 1. A value of 1 at a certain frequency means the signals are perfectly correlated and consequently no noise is interfering at that frequency. In addition to noise, coherence also measures how linear the relationship is as well as if other non-measured inputs are influencing the output.

The coherency spectra between the midboard flap and the pitch rate of the first chirp of flight 9a and 12 are shown in Fig. 4. During the first chirp the aircraft is only excited by the midboard flap. Hence, the system is only single input during that period. While flight 9a has large coherence values (above 0.8 for the interested frequency range), flight 12 exhibits bad coherence. Consequently, flight 12 will not be used for further identification. The reason behind the bad coherence is not fully understood and cannot be resolved, as the experiment cannot be repeated. The following points likely have contributed in various degrees to the bad coherence. Unlike during the other flights, the autothrottle controller could not hold the airspeed close to constant during the test segment. Specifically, the airspeed was oscillating between 24 m/s and 28 m/s. This speed change could have introduced nonlinear effects due to the change of dynamics with airspeed. Moreover, the amplitude of the chirp was reduced at higher frequencies in flight 12 to limit energy added to the lightly damped flexible mode. This naturally lead to a lower signal to noise ratio. This lower signal to noise could have deteriorated the quality of the data.

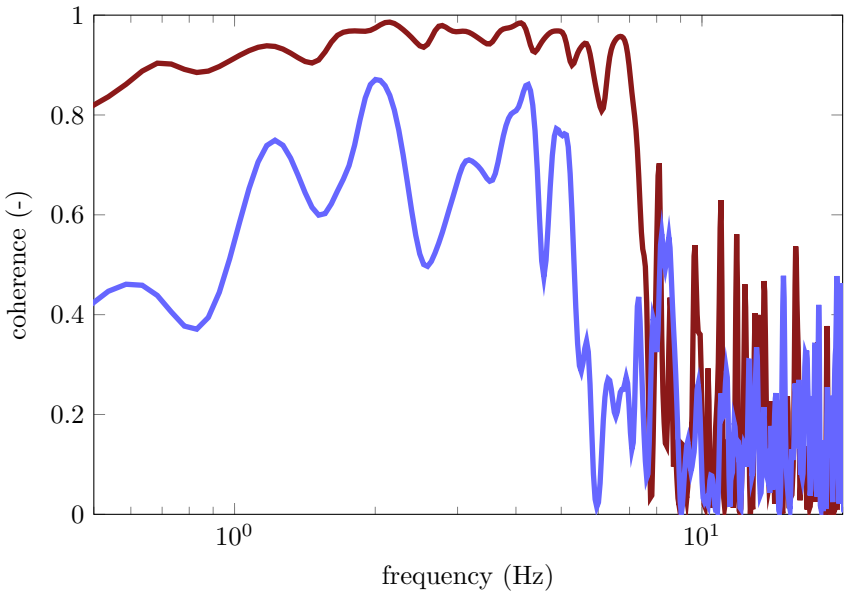

Figure 4. Coherency Spectrum of the Mid-Board Flap Chirp of Flight 9a (——) and Flight 12 (——)

V. Results of the System Identification

Due to the loss of aircraft at an early stage in the flight test campaign, only a limited data set is available for the parameter estimation. Hence, only a single flight data set will be used for the actual identification. Specifically, the parameters of the model structure presented in Section III are updated using the flight data of Sköll flight 9a, i.e. the chirp flight at 23 m/s. The remaining flight data will be used as validation data. In order to get a higher confidence in the identified model despite the limited data, different identification methods are used and the resulting models are compared.

A. Modal Identification

CFDD is used to obtain estimates for the prominent modes in both the flight data and from ground vibration test, which are used to obtain the structural dynamics of the parametric model. The results of the CFDD are given in Tab. 2. The modes and mode shapes identified by CFDD from the ground vibration test are used to set the C and D matrix of the parametric model, see Ref. 2. Additionally, the structural frequencies in the model are fixed to the identified values (i.e., first row in Tab. 2).

Several candidate modes were identified at each flight condition as shown in Tab. 2. Three of the most prominent flexible modes are presented as they displayed consistency between data points. These modes consist of first symmetric wing bending (SWB1), first asymmetric wing bending (AWB1), and second sym-

metric wing bending (SWB2). In addition to these modes, some of the flight test data points displayed a lower frequency mode that is believed to be the short period mode based on its frequency and identified mode shape. That mode is indicated in Tab. 2 if it was identified. CFDD performs well for lightly damped modes ($\zeta < 0.2$), therefore the damping estimate for the identified short period modes is questionable. The estimated short period frequency, however, is associated with high confidence.

Table 2. Flight test conditions

Flight Speed [m/s]	Short Period		SWB1		AWB1		SWB2	
	ω [rad/s]	ζ	ω [rad/s]	ζ	ω [rad/s]	ζ	ω [rad/s]	ζ
0	-	-	51.18	0.031	97.88	0.015	163.49	0.012
20	8.67	0.43	45.44	0.070	98.21	0.031	154.18	0.020
23	-	-	38.35	0.134	94.90	0.035	154.99	0.015
26	19.91	0.245	30.71	0.103	95.30	0.017	147.30	0.013

In Fig. 5, the power spectral density of the flight data recorded at flight 9 (i.e., at 23 m/s) is given. The red arcs in the figure indicate the location of the identified modes. As can be seen in the figure, the CFDD method is intended for identification of lightly damped mode, i.e. clearly distinguishable peaks in the spectrum. In general, the approach is more accurate in identifying the modal frequencies rather than the damping ratios. In addition, the naming of the mode shapes comes from the GVT which uses much more sensor signals (i.e., multiple accelerations along the wing). In the flight test, it is more difficult to classify the mode shapes due to the limited number of sensor signals.

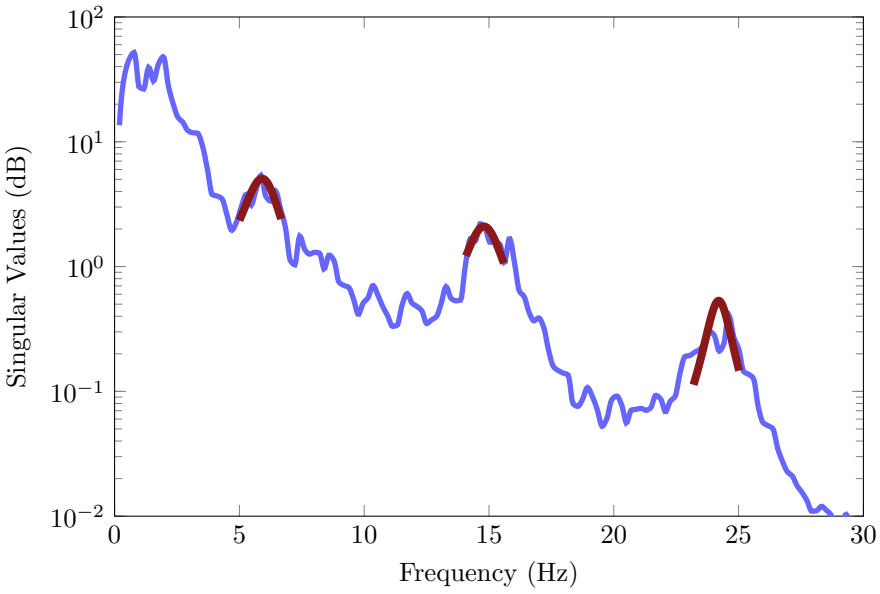

Figure 5. Power Spectral Density of Flight 9 ( ) with Identified Modes ( )

B. Parameter Estimation Results

The parameter estimation is performed using the `greyest` MATLAB function on the model structure presented in Section III. The time delay of the system is not directly optimized during the identification but is fixed a priori instead. In order to estimate the delay, black box LTI models with various time delays are identified using a subspace approach. The model that best matches the data is obtained by setting the delay to 40 ms on both input channels. This corresponds to four sampling steps. Having set the time delay, the prediction estimation error as described in Section II is minimized using `greyest`. The free parameters in

the optimization are dimensionless coefficients given in Equation (9). The resulting parameters after the optimization, as well as the initial values and bounds used in the optimization are summarized in Tab. 3.

Table 3. Parameter Estimation Results

Parameter:	$C_{M\alpha}$	C_{Mq}	$C_{M\delta_1}$	$C_{M\delta_2}$	$C_{M\eta_1}$	$C_{M\dot{\eta}_1}$
Optimal Value:	-0.263	-3.189	-0.232	-0.490	0.039	-0.286
Initial Value:	-0.175	-2.606	-0.229	-0.342	0.026	-0.571
Lower Bound:	-0.263	-3.909	-0.343	-0.513	0.013	-0.856
Upper Bound:	-0.088	-1.303	-0.114	-0.171	0.200	0.500
Parameter:	$C_{L\alpha}$	C_{Lq}	$C_{L\delta_1}$	$C_{L\delta_2}$	$C_{L\eta_1}$	$C_{L\dot{\eta}_1}$
Optimal Value:	5.154	5.797	0.279	0.664	-1.764	0.433
Initial Value:	4.887	5.777	0.539	0.443	-1.613	0.288
Lower Bound:	2.444	2.889	0.269	0.221	-2.419	0.144
Upper Bound:	7.331	8.667	0.808	0.664	-0.806	0.433
Parameter:	$C_{Q\alpha}$	C_{Qq}	$C_{Q\delta_1}$	$C_{Q\delta_2}$	$C_{Q\eta_1}$	$C_{Q\dot{\eta}_1}$
Optimal Value:	-1.979	-1.481	-0.032	-0.137	1.245	-0.854
Initial Value:	-0.662	-0.574	-0.011	-0.249	1.490	-0.337
Lower Bound:	-1.987	-1.722	-0.100	-0.747	0.298	-1.001
Upper Bound:	-0.133	-0.115	-0.002	-0.049	4.470	-0.067

A comparison of the quality of the initial model and the optimized one is given in Tab. 4. In addition to the quadratic norm of the prediction error as defined in Section II, the fitness value of the individual output channels is compared.[12] The fitness value f is defined by

$$f = 100\left(1 - \frac{\|y - \hat{y}\|}{\|y - \bar{y}\|}\right), \tag{11}$$

where y is the experimental data, $\hat{y}$ the predicted output and $\bar{y}$ the mean of the experimental data. A fitness value of 100 means that the model predicts the experimental data perfectly. A value of 0 means that the prediction is worse than using the mean value of the output as a prediction. The table not only give the values for flight 9a, which was used in the optimization, but also on the two validation sets, i.e. flight 9b and flight 3. Flight 3 is at a different flight speed. The dimensionless coefficients given in Tab. 3 are used to obtain models corresponding to this flight condition. As can be seen in the table, the parameter estimation provides a significant improvement in the model quality over the initial parameter values. The flight 3 data is the only set with a minor improvement.

Table 4. Error Metrics

	Fitness						Prediction Error	
	Pitch Rate		Center Accel.		Wing Tip Accel.			
	Initial	Optimal	Initial	Optimal	Initial	Optimal	Initial	Optimal
Flight 9a:	30.91	66.39	39.46	55.46	42.08	54.68	12.63	6.66
Flight 9b:	51.69	63.54	60.11	66.32	59.34	66.88	9.06	6.21
Flight 3:	67.55	63.47	57.63	58.92	64.17	67.59	6.38	5.63

In Fig. 6, the frequency response of all input and output channels is compared to the flight test data. The frequency response of the flight data is obtained by spectral analysis using the `spa` MATLAB function. An optimal width of the Hann window is chosen to minimize bias while still giving a smooth estimate, see Section II and Ref. 12. The frequency responses are also compared to a to a fourth order LTI model obtained by subspace identification, as described in Section II. The MATLAB function `n4sid` was used to get this model. A fourth order model was deemed sufficient, as an increase in order did not result in a significant

improvement of the accuracy of the identified model. As can be seen in Fig. 6, both the parameter estimation model and the subspace model match the measured frequency response in the interested frequency range, i.e. up to 50 rad/s. Beyond that frequency the aircraft dynamics were not excited during the experiment. Hence, the experimental data does not reliably capture the aircraft dynamics. The main difference between the black box model and the parametric model, is the inclusion of high frequency modes in the parametric model. Overall, the parametric model has order ten in comparison to four for the black box model. The additional modes, however, are not identified from flight data but stem from computational methods and ground tests. It can further be noted that the chosen delay of 40 ms in the inputs captures the phase loss in the frequency response data from the flight test very well.

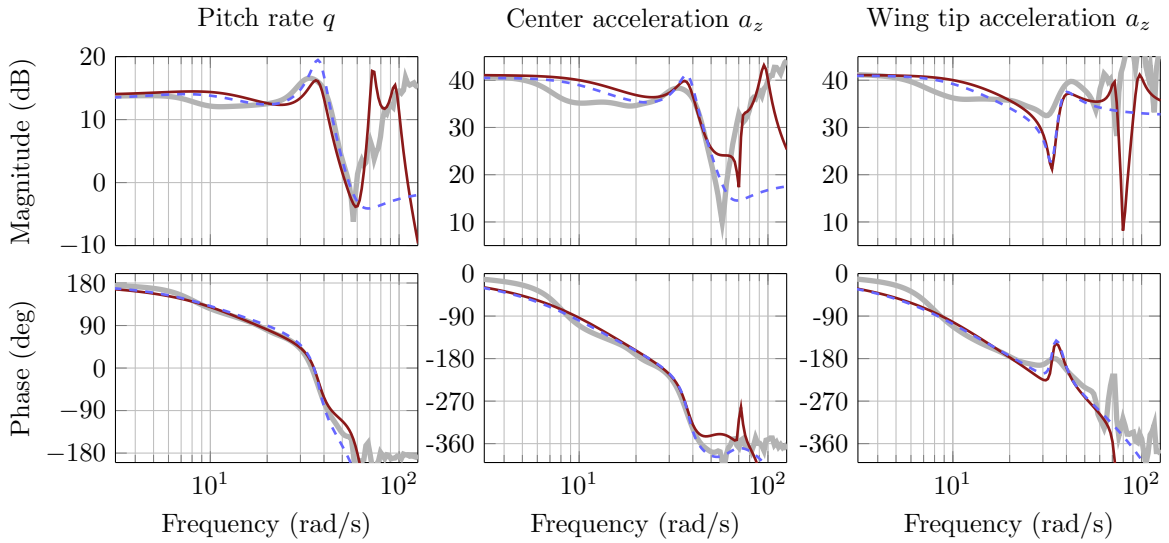

(a) Bode Diagrams from Midboard Flaps

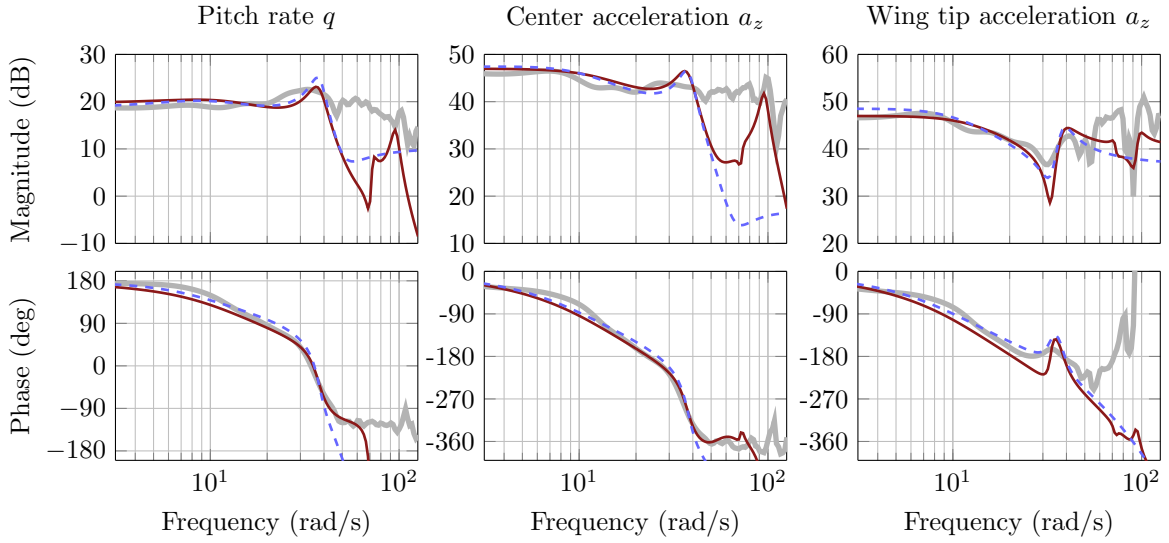

(b) Bode Diagrams from Outboard Flaps

Figure 6. Comparison of Frequency Responses from Flight Test (——), Subspace Identification (- - -) and Parameter Estimation (——) for Sköll Flight 9a

In order to validate the results of the parameter estimation on off-design flight data, the flights 9b and 3 are considered. Note that flight 3 is at a different airspeed, namely 20 m/s. The estimated dimensionless coefficients are used to obtain a model for this airspeed. In both data sets the aircraft was excited using 3-2-1-1 inputs on the flaps. As described earlier, these input signals are not well suited to capture the whole relevant frequency content. Still, with the limited data available they provide some validation data. A

comparison of the time responses from those two flight tests and the parametric model is shown in Fig. 7. As can be seen in the figure, the model matches the flight data accurately in both test cases.

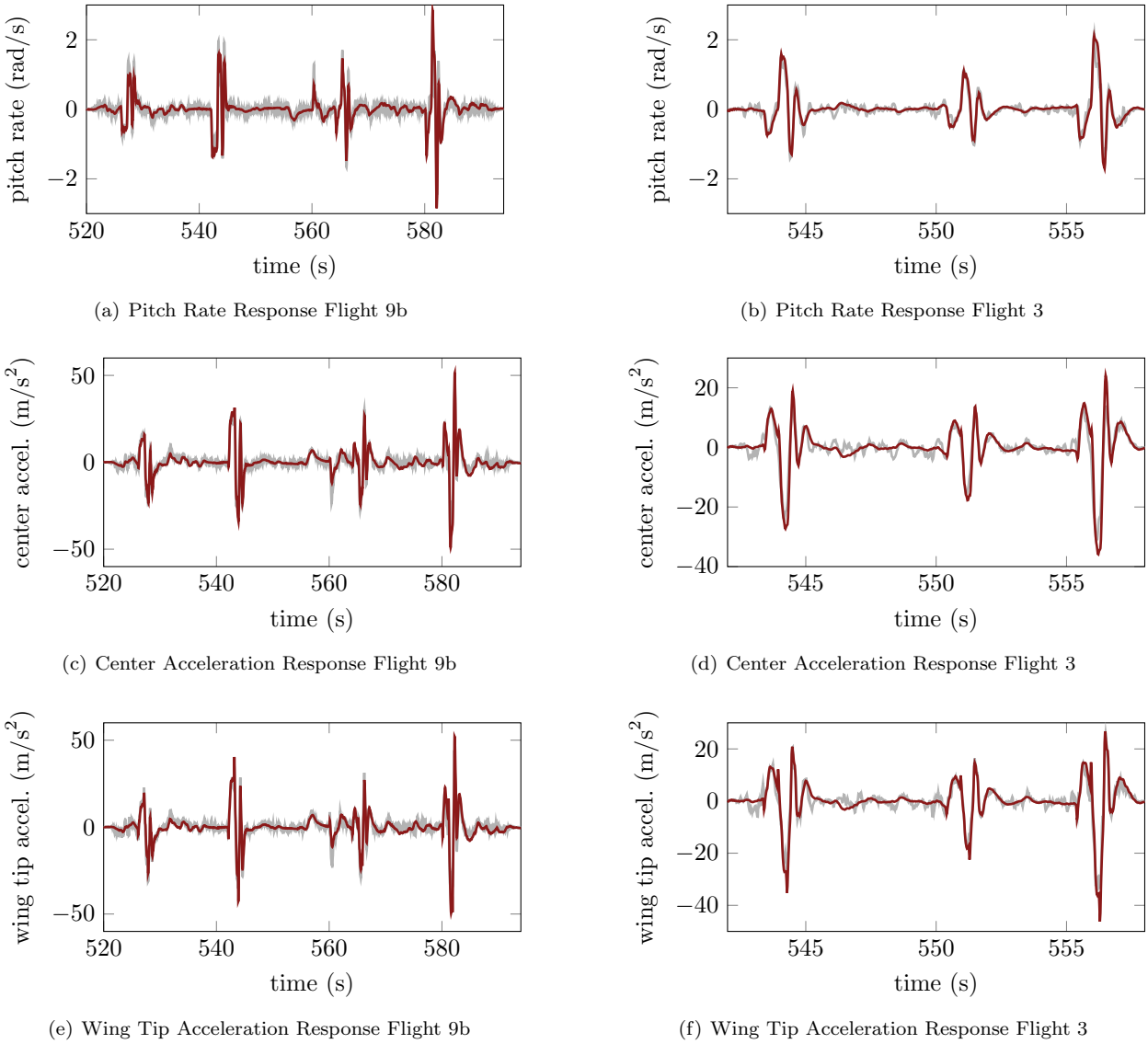

(a) Pitch Rate Response Flight 9b

(b) Pitch Rate Response Flight 3

(c) Center Acceleration Response Flight 9b

(d) Center Acceleration Response Flight 3

(e) Wing Tip Acceleration Response Flight 9b

(f) Wing Tip Acceleration Response Flight 3

Figure 7. Comparison of Time Responses from Flight Test (——) and Parameter Estimation (——)

As a final validation of the parametric model, its modes are compared to the modes identified by CFDD. The results of this comparison are given in Tab. 5, where CFDD denotes the results of the modal identification and PEST of the parameter estimation. The first symmetric wing bending mode of the parametric model matches the modes identified by CFDD well. As already mentioned in the previous section, the CFDD damping results for the short period mode are unreliable. Still, the frequencies are close to the ones of the parametric model. The parametric model has a flutter speed of 27.9 m/s, which is close to the approximate 30 m/s estimated in flight 13.

VI. Conclusion and Future Work

A flight test campaign was performed on a small flexible unmanned aircraft to obtain an adequate dynamical model for an ensuing control law design. During the identification campaign, the aircraft was excited both with 3-2-1-1 and chirp signals on its flaps at various flight conditions. The acceleration at the wing tip and center body and the pitch rate were measured. Based on the experimental data, the parameters

Table 5. Comparison of the Identified Modes

	Short Period				SWB1			
	ω [rad/s]		ζ		ω [rad/s]		ζ	
Flight Speed [m/s]	CFDD	PEST	CFDD	PEST	CFDD	PEST	CFDD	PEST
20	8.67	11.01	0.43	0.75	45.44	41.2	0.070	0.104
23	-	13.9	-	0.76	38.35	37.3	0.134	0.101
26	19.91	17.7	0.245	0.804	30.71	32.7	0.103	0.061

of an initial model of the flexible aircraft were updated. The results of the parameter estimation were validated using standard techniques from system identification, as well as by comparison with different system identification techniques, namely subspace identification and curve fitting frequency domain decomposition. All validation methods show that the estimated parameters capture the aircraft dynamics adequately.

As the flight test campaign was cut short due to the loss of the aircraft, future work will include a more thorough campaign on a newly built aircraft with similar characteristics. In this future campaign additional candidate input type will be considered, e.g., orthogonal multi-sines or pseudo random signals.

Acknowledgments

The authors would like to remember our lost friend Dr. Gary Balas, who initiated this research project and was the original principle investigator. This work is supported by the NASA NRA Cooperative Agreement under Grant No. NNX14AL36A, entitled "Lightweight Adaptive Aeroelastic Wing for Enhanced Performance Across the Flight Envelope". Mr. John Bosworth is the Technical Monitor.

References

[1]Theis, J., Pfifer, H., and Seiler, P., "Robust Control Design for Active Flutter Suppression," *AIAA Scitech Conference*, 2016.

[2]Schmidt, D. K., Zhao, W., and Kapania, R., "Flight Dynamics and Flutter Modeling and Analysis of a Flexible Flying-Wing Drone," *AIAA Scitech Conference*, 2016.

[3]Waszak, M. R. and Schmidt, D. K., "Flight Dynamics of Aeroelastic Vehicles," *Journal of Aircraft*, Vol. 25, 1988, pp. 563–571.

[4]Schmidt, D., *Modern Flight Dynamics*, McGraw-Hill, New York, 2012.

[5]Schulze, C., Thompson, P. M., Danowsky, B. P., Lee, D., and Harris, C., "System Identification and Modal Extraction from Response Data," *AIAA Atmospheric Flight Mechanics Conference*, No. 2013-4919, 2013.

[6]Jategaonkar, R. V., Fischenberg, D., and Gruenhagen, W., "Aerodynamic modeling and system identification from flight data-recent applications at dlr," *Journal of Aircraft*, Vol. 41, No. 4, 2004, pp. 681–691.

[7]Klein, V. and Morelli, E. A., *Aircraft system identification: theory and practice*, American Institute of Aeronautics and Astronautics, 2006.

[8]Tischler, M. B. and Remple, R. K., "Aircraft and rotorcraft system identification," *AIAA Education Series. American Institute of Aeronautics and Astronautics, New York*, 2006.

[9]Theodore, C., Ivler, C. M., Tischler, M. B., Field, E., Neville, R., and Ross, H., "System Identification of Large Flexible Transport Aircraft," *AIAA Atmospheric Flight Mechanics Conference*, No. 2008-6894, 2008.

[10]de Oliveira Silva, B. G., "Data Gathering and Preliminary Results of the System Identification of a Flexible Aircraft Model," *AIAA Atmospheric Flight Mechanics Conference*, No. 2011-6355, 2011.

[11]de Oliveira Silva, B. G. and Mönnich, W., "System Identification of Flexible Aircraft in Time Domain," *AIAA Atmospheric Flight Mechanics Conference*, 2012.

[12]Ljung, L., *System Identification*, Springer, 1998.

[13]Bendat, J. S. and Piersol, A. G., *Engineering Applications of Correlation and Spectral Analysis*, Vol. 1, John Wiley and Sons, 1980.

[14]Brincker, R., Zhang, L., and Andersen, P., "Modal identification from ambient responses using frequency domain decomposition," *International Modal Analysis Conference*, 2000.

[15]Brincker, R., Ventura, C., and Andersen, P., "Damping estimation by frequency domain decomposition," *19th International Modal Analysis Conference*, 2001, pp. 698–703.

[16]Van Overschee, P. and De Moor, B., "N4SID: Subspace algorithms for the identification of combined deterministic-stochastic systems," *Automatica*, Vol. 30, No. 1, 1994, pp. 75–93.

[17]Burnett, E., Atkinson, C., Beranek, J., Holm-Hansen, B., and Nicolai, L., "NDOF Simulation model for flight control

development with flight test correlation," *AIAA Modeling and Simulation Technologies Conference, Toronto, Canada*, 2010, pp. 7780–7794.

[18]Gupta, A. and Seiler, P., "Ground Vibration Test on Flexible Flying Wing Aircraft," *AIAA Scitech Conference*, 2016.

[19]Moreno, C., Gupta, A., Pfifer, H., Taylor, B., and Balas, G., "Structural Model Identification of a Small Flexible Aircraft," *American Control Conference*, 2014, pp. 4379–4384.